How to cite: Angew. Chem. Int. Ed. 2025, e202425049
doi.org/10.1002/anie.202425049

Hydrogen Bonding

Where Does the Proton Go? Structure and Dynamics of Hydrogen-Bond Switching in Aminophosphine Chalcogenides

*Tanja Huber, Gabriel Mayer, Manuel Kümper, Wagner Silva, Nicolò Fontana, Alexander Falk, Simon H. F. Schreiner, Johannes Gramüller, Alexander Scrimgeour, Emily Groß, Ruth M. Gschwind, Dominik Horinek, Patrick Nuernberger, and Jonathan O. Bauer**

Abstract: Aminophosphates are the focus of research on prebiotic phosphorylation chemistry. Their bifunctional nature also makes them a powerful class of organocatalysts. However, the structural chemistry and dynamics of proton-binding in phosphorylation and organocatalytic mechanisms are still not fully understood. Aminophosphine chalcogenides, preserving the central $H_2N–P^+–Ch^-$ structural motif, represent well-suited molecular models that mimic proton-binding, hydrogen-bond switching and supramolecular self-assembling behavior of catalytically and prebiotically relevant molecules. Through spectroscopic (IR, ^1H DOSY, ^{15}N NMR), molecular dynamics, and computational investigations, the dynamic proton switching capability of aminophosphate analogs was demonstrated. It was shown under which conditions the amino (NH_2) or chalcogen (Ch) functions in $H_2N–P^+–Ch^-$ structural units are protonated. In fact, all conceivable modes of hydrogen-bonding were identified, revealing substantial differences between the oxygen derivative and the heavier congeners. Using coordinating anions, supramolecular zigzag- and cube-shaped arrangements were found in the solid-state and in solution. After break-up of the cube structure, the sulfides and selenides no longer form stable interactions with HCl molecules. In the absence of coordinating anions, however, protonation of the chalcogen function is preferred. In contrast to the oxygen derivative, the heavier protonated congeners show dynamic intramolecular proton-hopping between the chalcogen and the amino function.

Introduction

Hydrogen-bonds are crucial for the stabilization of intermolecular interactions in biological systems, in catalysis, and in supramolecular self-organization processes.[1] The understanding of hydrogen-bond interactions has also profoundly influenced the field of catalysis.[2] BINOL-derived (thio)phosphoric acids[3] and phosphoramides[4] are among the most prominent organocatalysts for a variety of asymmetric transformations (Figure 1, A). For such systems, it turned out that the mechanistic picture is much more complex than one might assume and that the interplay of hydrogen-bonding and ion-pairing is of significant importance for the actual mode of activation.[5] Phosphine sulfides (R_3PS) themselves are also increasingly used in catalysis,[6] find application as synthetic intermediates[7] and in functional materials,[8,9] and are an integral part of the design of new types of ligands.[10] Furthermore, recent work has highlighted the prominent role of phosphonium chalcogenides, particularly selenium derivatives, in the field of chalcogen-bonding catalysis, a rapidly emerging new concept in organocatalysis (Figure 1, B).[11]

Another research area in which phosphate species have received particular attention is the chemistry of prebiotic systems.[12] Especially aminophosphates exhibiting the bifunctional structural motif $H_2N–P^+–O^-$ have long been the focus of interest in origin of life studies, as they are considered plausible and efficient prebiotic phosphorylation reagents in aqueous environments (Figure 1, C).[12,13] In this context, also thiophosphate (PSO_3^{3-}) has been found to be a potent prebiotic reagent[14] and just recently, a photochemical process has been proposed as a possible source of thiophosphate on the early Earth.[15]

However, given the importance of hydrogen-bonding pattern and proton transfer processes involving phosphorus-

[*] Dr. T. Huber, M. Kümper, Dr. N. Fontana, A. Falk, S. H. F. Schreiner, PD Dr. J. O. Bauer
Faculty of Chemistry and Pharmacy, Institute of Inorganic Chemistry
University of Regensburg
Universitätsstraße 31, D-93053 Regensburg, Germany
E-mail: jonathan.bauer@ur.de

G. Mayer, A. Scrimgeour, E. Groß, Prof. Dr. D. Horinek, Prof. Dr. P. Nuernberger
Faculty of Chemistry and Pharmacy, Institute of Physical and Theoretical Chemistry
University of Regensburg
Universitätsstraße 31, D-93053 Regensburg, Germany

Dr. W. Silva, Dr. J. Gramüller, Prof. Dr. R. M. Gschwind
Faculty of Chemistry and Pharmacy, Institute of Organic Chemistry
University of Regensburg
Universitätsstraße 31, D-93053 Regensburg, Germany

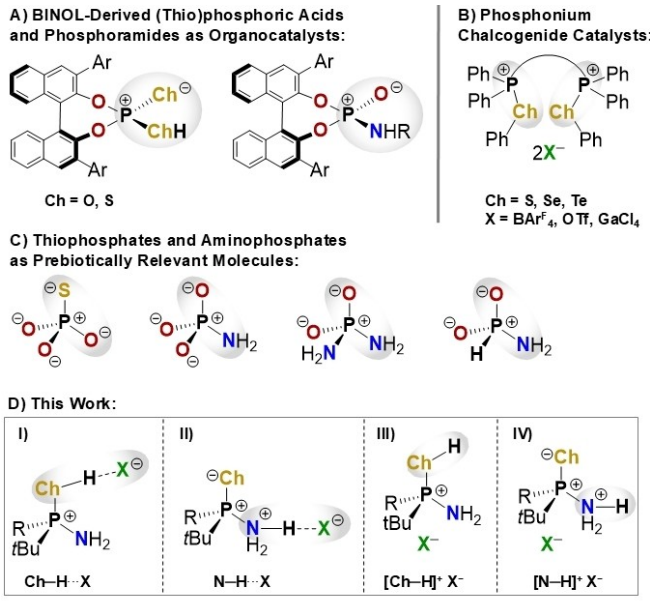

Figure 1. Phosphorus-chalcogen and phosphorus-amino subunits as key functions in A) BINOL-based (thio)phosphoric acids and phosphoramides for use in hydrogen-bond catalysis, in B) phosphonium chalcogenides that find application in chalcogen-bond catalysis, and in C) molecules that are considered crucial for prebiotic phosphorylation processes. D) This work: Aminophosphine chalcogenides investigated herein as well-suited bifunctional model systems for mimicking catalytically important and prebiotically relevant phosphate species. General principles of hydrogen-bonding modes and proton-binding scenarios depending on the type of counteranion. R = *t*Bu, Cy; X^- = coordinating or weakly coordinating anion

containing compounds in prebiotic scenarios,[12–15] in biological systems,[16] and in catalysis,[17] the role of phosphate species in proton-binding and hydrogen-bonding is still poorly understood. Just recently, it was shown that the ability of phosphate-based Brønsted acid catalysts to bind substrates in a mono- or bidentate fashion has a crucial influence on the pathways of the catalytic reaction and the stereoselectivities.[18] The need for a better understanding of proton-binding in phosphate species is also particularly justified by the fact that the protonation of aminophosphates and thus the pH dependence was found to play an essential role in prebiotic phosphorylation mechanisms.[19] In this context, the question of whether the oxygen or nitrogen function is protonated has long been debated.[20]

Phosphonates and phosphine chalcogenides are well-suited organic phosphorus derivatives that can mimic prebiotic, biological, and catalytically important phosphate molecules by restricting the structural pattern to crucial functional motifs.[21] Feringa et al. for example,[21d] recently presented a plausible chiral amplification scenario based on hydrogen-bonding between the P^+–O^- and N–H functions of aminophosphates and highlighted the possible role of phosphorylated amino acids in the emergence of prebiotic homochirality.[22]

We therefore focus here on aminophosphine chalcogenides [$(R_2P(Ch)(NH_2)$], which are organic derivatives of aminophosphates (Figure 1, D). They preserve the central H_2N–P^+–Ch^- function, whose potential and relevance for organocatalysis and the chemistry of prebiotic systems has recently already been recognized.[21d,e,23,24] Both functional units, the amino group (NH_2) and the phosphorus chalcogenide group (P^+–Ch^-, Ch = O, S, Se), are in principle capable of proton-binding and can therefore act as binding sites in hydrogen-bonded assembling processes and organocatalysis (Figure 1, D).[23] Studying structure and dynamics of proton transfer and hydrogen-bonding modes in the presence of coordinating and weakly interacting counteranions can provide fundamental insights into the functioning of molecular switches.[25] However, a systematic investigation of the counteranion-dependent protonation and hydrogen-bond switching capability of the fundamentally important bifunctional H_2N–P^+–Ch^- structural motif has not yet been undertaken. Our investigation is the first to systematically address the structural chemistry and dynamics of proton-binding in aminophosphate analogs in the presence of different counteranions to answer the question of how the two competing acceptor atoms (N, Ch) are involved in hydrogen-bonding both in the solid-state and in solution, and to reveal under which conditions the protonation of one of the two binding sites is preferred. Our approach consisted of a combination of various spectroscopic methods (IR, ^{1}H DOSY, ^{15}N NMR), density functional theory (DFT) calculations, molecular dynamics (MD) simulations and crystallographic analyses, and also considered the implications of stereochemistry on the formation of homochiral hydrogen-bonded assemblies. The results of this investigation are of fundamental importance for our understanding of protonation in prebiotic systems as well as for the design of new bifunctional catalyst systems based on hydrogen- and chalcogen-bonding.

Results and Discussion

Ch–H···X Versus N–H···X Hydrogen-Bonding

We have structured our discussion in such a way that we first consider the structures in the solid-state in detail before expanding our view to an in-depth analysis of the structural and dynamic behavior in solution.

The molecules investigated were the achiral di-*tert*-butylaminophosphine oxide (**1**), sulfide (**2**), and selenide (**4**) as well as the *P*-stereogenic (*tert*-butyl)cyclohexylaminophosphine sulfide in its racemic [(*rac*)-**3**] and enantiomerically pure form [(R_P)-**3**]. The latter was synthesized according to our recently established method to provide *P*-stereogenic aminophosphine sulfides.[26] All precursors were subjected to protonation with excess hydrogen chloride in diethyl ether at room temperature, the HCl adducts [**1**·HCl]$_n$, [**2**·HCl]$_4$, [(R_P)-**3**·HCl]$_4$, [(*rac*)-**3**·HCl]$_4$, and [**4**·HCl]$_4$ being obtained as single-crystalline solids (Scheme 1).

Single-crystal X-ray diffraction analysis of compound [**1**·HCl] (Figure 2) showed protonation of the P^+–O^- unit

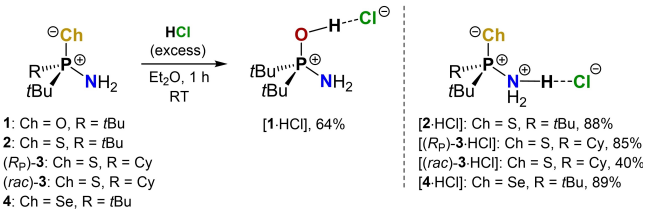

Scheme 1. Synthesis of hydrogen chloride adducts of aminophosphine chalcogenides (Ch = O, S, Se).

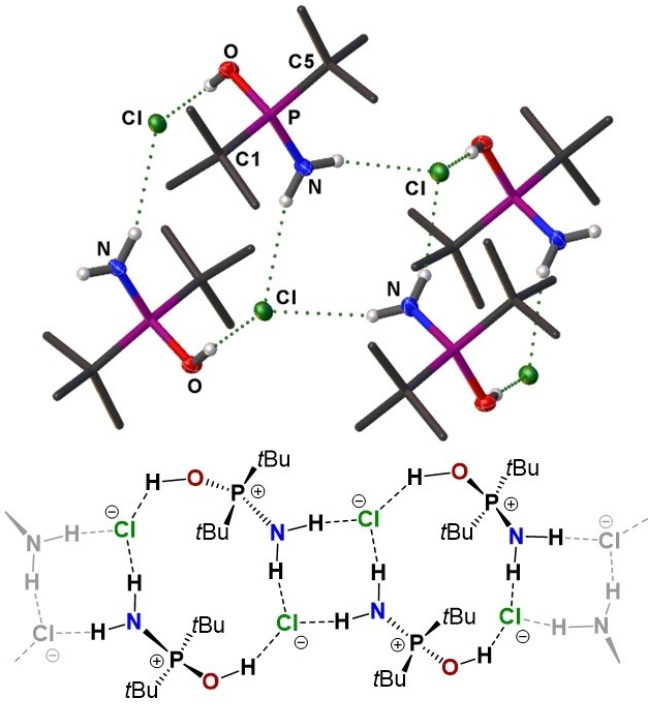

Figure 2. Part of the two-dimensional, zigzag-like molecular chain structure in the crystal structure of the hydrogen chloride adduct $[\mathbf{1}\cdot HCl]_n$ (Ch = O) (displacement ellipsoids are set at the 50% probability level). Hydrogen atoms, except for the OH and NH_2 groups, are omitted for clarity.[27]

and thus expression of the **Ch**–H···X (Ch = O, X = Cl) hydrogen-bond motif (**I** in Figure 1, D).[27] However, since both the OH and NH_2 groups participate in hydrogen-bonding to the chloride ion, a two-dimensional chain structure $[\mathbf{1}\cdot HCl]_n$ in a zigzag-like shape is formed with N···Cl distances of 3.257 Å and 3.312 Å and an O···Cl distance of 2.921 Å. The overall structure exhibits a "sandwich" profile, consisting of an "inner", polar hydrogen-bond network lying between non-polar layers formed by the *tert*-butyl groups. These individual layers are held together via dispersion interactions between the aliphatic groups. A detailed examination of the interaction pattern in the crystal structure of $[\mathbf{1}\cdot HCl]_n$ also revealed that attractive C–H···Cl contacts could play a supporting role in the formation of the hydrogen-bonded chain structure (for details on crystal structure analysis, see the Supporting Information, SI).

In contrast to the oxygen case (see Figure 2), in the solid-state structures of the sulfides [**2**·HCl], $[(R_P)$-**3**·HCl], and [(*rac*)-**3**·HCl] as well as the selenide [**4**·HCl] (Figure 3), the **N**–H···X (X = Cl) hydrogen-bond motif is expressed (**II** in Figure 1, D).[27] The four crystal structures each consist of hydrogen-bonded tetramers with a cubic core whose corners are alternately occupied by ammonium and chloride ions. The tetranuclear hydrogen-bonded units of the heavier congeners interact with each other through the largely non-polar outer regions (i.e. the *tert*-butyl and chalcogen functions) through both dispersive and Ch···H–C interactions. All cubes, except for the racemic case, show T_d symmetry. The asymmetric unit of the crystal structure of $[(rac)\text{-}\mathbf{3}\cdot HCl]_4$ contains two types of heterochiral, diastereomorphic cubic tetramers with the racemic composition (S_P,S_P,R_P,R_P) and the enantiomerically enriched composition (S_P,S_P,S_P,R_P). The two diastereomeric cube formations in the asymmetric unit are held together by dispersive and Ch···H–C interactions between molecular fragments of the same configuration at phosphorus $[(S_{P4})\cdots(S_{P5})/(R_{P3})\cdots(R_{P6})]$. Viewed in the light of the homochiral tetramer $[(R_P)\text{-}\mathbf{3}\cdot HCl]_4$ with the composition (R_P,R_P,R_P,R_P), which was formed from an enantiomerically pure sample, the appearance of molecular hydrogen-bonded aggregates enriched in one enantiomer is a remarkable finding with respect to the emergence of

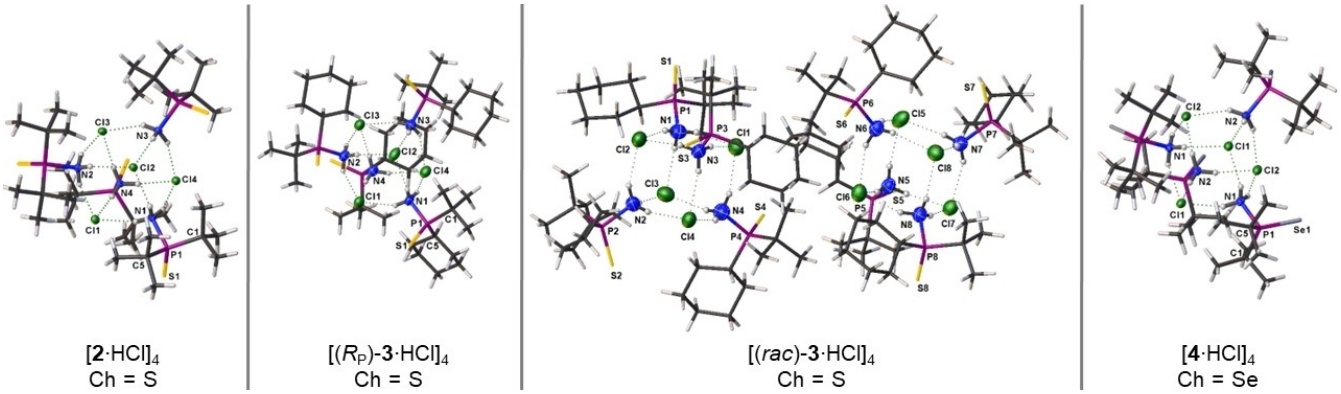

Figure 3. Cubic supramolecular assemblies in the crystal structures of the hydrogen chloride adducts $[\mathbf{2}\cdot HCl]_4$, $[(R_P)\text{-}\mathbf{3}\cdot HCl]_4$, $[(rac)\text{-}\mathbf{3}\cdot HCl]_4$, and $[\mathbf{4}\cdot HCl]_4$ (displacement ellipsoids are set at the 50% probability level).[27]

homochirality and chiral self-recognition mechanisms in supramolecular assemblies.[21d,e,22] DFT calculations [M062X/6−31+G(d)][28–30] of the three separate diastereomorphic cubes using the polarizable continuum model (PCM)[31] (solvent: dichloromethane, DCM) showed a significant gradation of the Gibbs energies (ΔG) of the solvated cubes in the order (R_P,R_P,R_P,S_P) (0 kJ mol^{-1}) < (R_P,R_P,R_P,R_P) (4 kJ mol^{-1}) < (R_P,R_P,S_P,S_P) (14 kJ mol^{-1}) with a clear energetic preference for the two scalemic tetramers. Above all, it is clear that the P$^+$–Ch$^-$ units (Ch = S, Se) of the cubane-like supermolecules [**2**·HCl]$_4$, [(R_P)-**3**·HCl]$_4$, [(*rac*)-**3**·HCl]$_4$, and [**4**·HCl]$_4$ remain unprotonated in the solid-state. Instead, the three hydrogen atoms of each NH_3 unit point along the edges of the cube toward a chloride acceptor.

In the case of aminophosphine sulfides and selenides, only the amino functions are involved in the assembly process, provided the counteranion is capable of hydrogen-bonding. Apparently, in case of N–P$^+$–S$^-$ and N–P$^+$–Se$^-$ pattern, an ammonium ion-based hydrogen-bonded cube assembly appears to benefit from a significant energy gain over protonation of the phosphine chalcogenide moiety that occurs in case of an N–P$^+$–O$^-$ pattern.

Molecular cubic clusters held together exclusively by hydrogen-bonds[32] are particularly interesting in terms of spontaneous self-assembly and they are often thought to act as shape-determining building blocks for the formation of larger superstructures.[33] Protonated primary amines have always played an important role in cubic assemblies because they can form a three-dimensional network by incorporation of all three hydrogen atoms, provided appropriate hydrogen-bonding acceptor atoms are present.[34] However, so far, all hydrogen-bonded cubane-like arrangements known from the literature lack functional groups in the periphery of the cubic core and are therefore limited in their expandability. Besides that, only little is known about the solution structures of fundamental inorganic functional pattern concerning their involvement in different hydrogen-bond motifs.

To get insight into the structures of these basic functional molecules in solution, we performed ^{1}H-diffusion-ordered NMR spectroscopic (^{1}H DOSY) measurements[35] of the previously isolated supermolecules [**1**·HCl]$_n$, [**2**·HCl]$_4$, [(R_P)-**3**·HCl]$_4$, and [**4**·HCl]$_4$ in DCM at room temperature with different concentrations.

Beginning with the heavier congeners (Ch = S, Se), the hydrodynamic volume of compound [**2**·HCl] increased continuously from 435 Å^3 (30 mM) to 670 Å^3 (50 mM) to 905 Å^3 (100 mM), the latter has about four times the volume of the non-protonated monomeric reference molecule **2** (248 Å^3). To exclude possible hydrogen-bonding interactions between the amino and sulfur moieties of compound **2** itself, di-*tert*-butylchlorophosphine sulfide was used as an additional reference molecule, for which a quite similar volume of 228 Å^3 was obtained. These results clearly indicate an increasing tetrameric association with increasing concentrations also in DCM solution and correspond well with a cubic synthon composition like [**2**·HCl]$_4$ as found in the crystal structure (see Figure 3). The same conclusion can be drawn for the homochiral, enantiomerically pure cube [(R_P)-**3**·HCl]$_4$ (for details, see the SI, Table S1). For the HCl adduct of the selenium derivative [**4**·HCl], a higher concentration of 500 mM was required for an almost complete formation of a tetrameric assembly [**4**·HCl]$_4$. The hydrodynamic volume of 855 Å^3 is in turn about four times larger than the volume of the respective non-protonated reference molecule (**4**: 235 Å^3). Reducing the concentration of compounds [**2**·HCl]$_4$, [(R_P)-**3**·HCl]$_4$, and [**4**·HCl]$_4$ to 5 mM resulted in the formation of a solution species that is clearly indicative of a monomer according to the measured hydrodynamic volumes of 265 Å^3, 273 Å^3, and 251 Å^3, respectively.

Concentration-dependent and variable temperature ^{1}H and ^{31}P NMR spectroscopy of the sulfur- and selenium-based compounds [**2**·HCl] and [**4**·HCl] are consistent with the results of the ^{1}H DOSY measurements (for details, see the SI). In the ^{31}P NMR spectrum of [**2**·HCl], two defined species can be identified when the concentration increases or the temperature decreases (Figure 4, top, right). The ^{31}P NMR signal of δ = 94.2 ppm at 5 mM (DCM) and 298 K differs only slightly from the free molecule **2** [δ(^{31}P) = 94.1 ppm]. Under these conditions, fully in agreement with the DOSY results, only a monomeric species is present, which apparently does not form a stable bond to an HCl molecule (therefore referred to as **2**$_{HCl}$ in the following). As the concentration increases (condition **A**, Figure 4) or the temperature decreases (condition **B**, Figure 4), the formation of a second species at the expense of **2**$_{HCl}$ can be increasingly recognized, to which a significantly downfield-shifted ^{31}P NMR signal of δ = 111.5 ppm can be assigned. When viewed together with the DOSY measurements, this second species can clearly be identified as the cubic aggregate [**2**·HCl]$_4$. The latter seems to be exclusively present in a 100 mM DCM solution at 298 K. In a 10 mM DCM solution, compound [**2**·HCl]$_4$ can be identified as the sole species at temperatures below 273 K. Here too, the lower tendency of the selenium congener to aggregate is evident: When the temperature decreases for a 10 mM DCM solution of [**4**·HCl], the ^{1}H and ^{31}P NMR signals for the P–NH_2 group of **4**$_{HCl}$ can still be clearly observed even at 193 K (see the SI, Figures S104 and S105).

The increasing formation of cube [**2**·HCl]$_4$ with increasing concentration can also be monitored using infrared (IR) spectroscopy (Figure 4, top, left). The difference IR absorption spectra normalized to the concentration in DCM showed that the intensity of the broad band at 2750 cm^{-1} (N–H stretching vibration of the NH_3 groups) increases from 10 mM to 100 mM. Furthermore, for cube [**2**·HCl]$_4$, the strongly downfield-shifted ^{1}H NMR signal at δ(^{1}H) = 9.56 ppm can be clearly assigned to the P–NH_3 group. The ^{1}H NMR signal of **2**$_{HCl}$ (5 mM in DCM, 298 K) at δ = 2.14 ppm is, however, in the same chemical shift region as the P–NH_2 group of the free molecule **2** (δ = 2.20 ppm), surprisingly indicating a free, non-protonated amino group in case of **2**$_{HCl}$. In agreement of this, the IR spectra of species **2**$_{HCl}$ and the free reference compound **2** in DCM are also almost identical (for details, see the SI, Figure S107).

Definitive evidence of the P–NH_2 group of compound **2** being virtually unaffected by HCl at low concentrations is

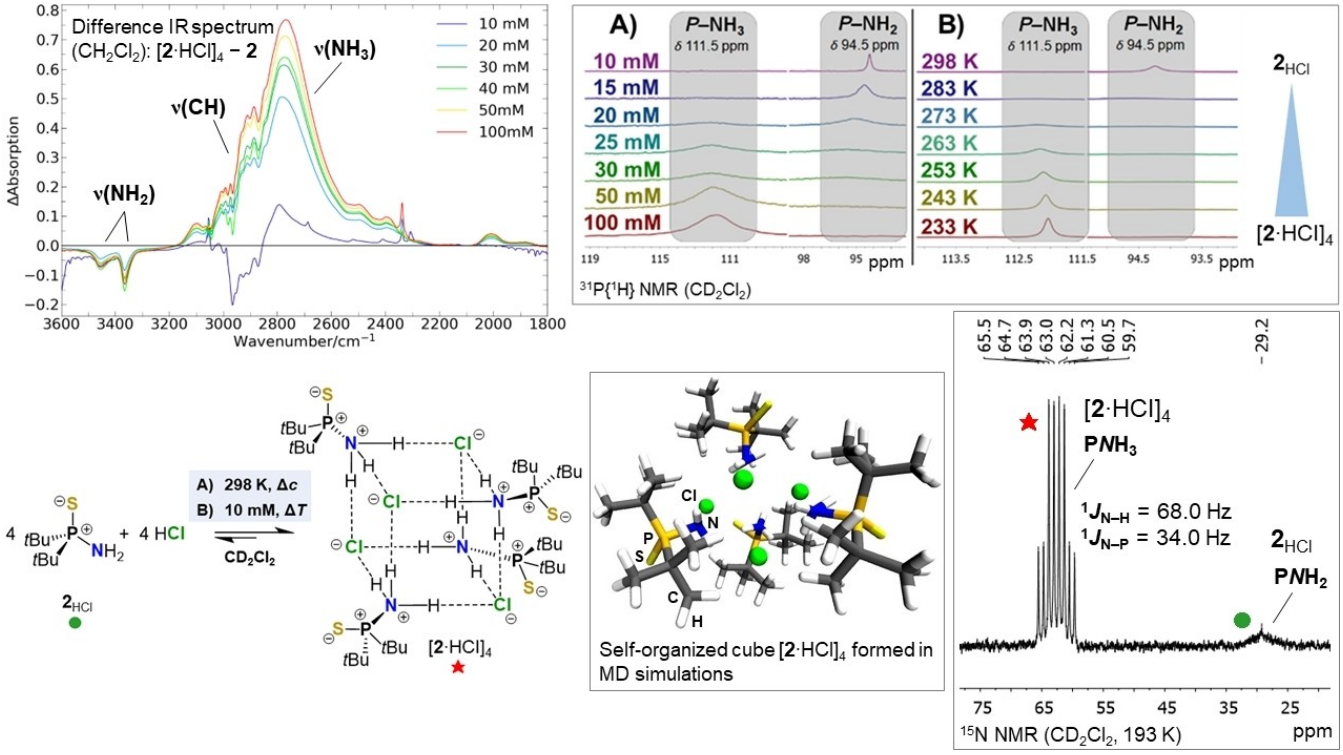

Figure 4. Investigation of the self-assembly process of aminophosphine sulfide $\mathbf{2}_{HCl}$ to the cubic supermolecule [**2**·HCl]$_4$ in DCM solution. Evidence of a total loss of stable interactions between compound **2** and HCl when the concentration decreases or the temperature increases. Top, left: Difference IR spectrum ([**2**·HCl]$_4$ – **2**) normalized to different concentrations. Top, right: Concentration-dependent (**A**) and variable temperature ^{31}P NMR spectroscopy (**B**) of the association process. Bottom, right: ^{15}N NMR spectroscopy of [**2**·HCl] (100 mM) to clearly identify the association mode of compound **2** in the presence of hydrogen chloride in solution. Bottom, middle: The self-assembling process toward the cube aggregate [**2**·HCl]$_4$ could be followed by MD simulations.

provided by ^{15}N NMR spectroscopy. The ^{15}N NMR spectrum of ^{15}N-labeled, free **2** shows a triplet of doublets at $\delta =$ 29.1 ppm with $^1J_{N-P} = 22.2$ Hz and $^1J_{N-H} = 76.0$ Hz (see also Figure 8, later in the discussion). The $^1J_{N-H}$ coupling constant of aminophosphine sulfide **2** can even be interpreted as a clear indication of a pyramidal geometry around the nitrogen atom of the P–NH$_2$ group.[36] Although the $^1J_{N-H}$ coupling of $\mathbf{2}_{HCl}$ (5 mM in DCM, 298 K) is only weakly resolved due to the low concentration, the chemical shift [$\delta(^{15}N) = 29.0$ ppm] and the $^1J_{N-P}$ coupling constant (22.4 Hz) obtained from the ^{1}H-decoupled ^{15}N{^{1}H} NMR spectrum are almost identical to that of the free molecule **2**. ^{15}N NMR spectroscopy at 193 K of the ^{15}N-labeled tetramer [**2**·HCl]$_4$ (100 mM) shows an excellently resolved and significantly downfield-shifted quartet of doublets at $\delta = 62.6$ ppm with $^1J_{N-P} = 34.0$ Hz and $^1J_{N-H} = 68.0$ Hz, which is clear evidence of an sp^3-hybridized and protonated nitrogen atom in the form of a P–NH$_3$ group.[36] This signal is accompanied by a small, broadened triplet at 29.0 ppm belonging to a small equilibrium amount of $\mathbf{2}_{HCl}$ (Figure 4, bottom, right). In fact, ^{15}N NMR spectroscopy unambiguously proves the protonation of only the NH$_2$ function of the heavier phosphine chalcogenides (Ch = S, Se) and indicates a rigid and tight hydrogen-bonded association of four [**2**·HCl] units to a [**2**·HCl]$_4$ aggregate in solution that most closely matches a cube structure as found in the solid-state. The experimental finding of tetrameric cube-shaped aggregates in DCM solution was impressively confirmed in molecular dynamics (MD) simulations, in which the according structures (Figure 4, bottom, middle) emerge after starting from a random distribution of reactants. Since the results from experiments and computations are fully consistent, the cubic supermolecule [**2**·HCl]$_4$ is clearly identified as the stable form of the HCl adducts in the case of the heavier congeners.

At this point, however, the exciting question arises as to what the oxygen congener [**1**·HCl] actually looks like in solution. Here too, an increasing association can be clearly seen in ^{1}H DOSY measurements as the concentration increases from a 0.2 mM to a 200 mM DCM solution at 298 K (Figure 5, top, left). In the same direction, the hydrodynamic volume increases from 278 Å^3 to 890 Å^3 and therefore asymptotically approaches a value that is approximately four times the volume of a monomeric species. Remarkably, with increasing concentration, the ^{31}P NMR signal of compound [**1**·HCl] undergoes a downfield shift from 68.3 ppm (2 mM) to 71.3 ppm (200 mM) at 298 K (Figure 5, top, right). For comparison, the ^{31}P NMR signal of free **1** appears at 55.2 ppm with $^1J_{N-P} = 15.7$ Hz. This already indicates a transition from a monomeric HCl adduct [**1**·HCl] at very low concentrations to a higher degree of aggregation, presumably in the form of a tetrameric species. Could this also be due to the formation of a cube structure analogous

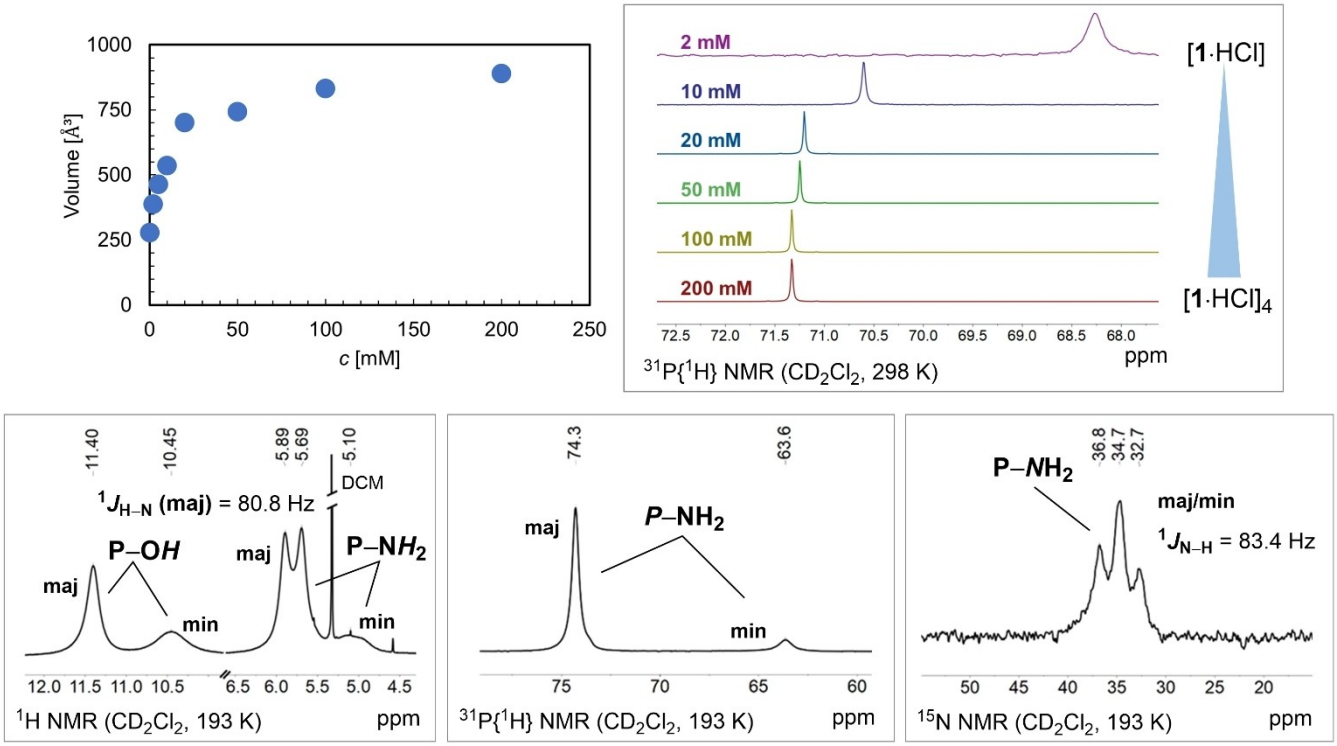

Figure 5. Investigation of the supramolecular chemistry of the HCl adduct [**1**·HCl]. Top, left: ^{1}H DOSY measurements at 298 K to investigate the self-assembly behavior of [**1**·HCl] in DCM solution in the range of 0.2 mM and 200 mM. Top, right: Concentration-dependent ^{31}P NMR spectroscopy to support the existence of stable interactions between compound **1** and HCl even at very low concentrations. Bottom: ^{1}H, ^{31}P{^{1}H}, and ^{15}N NMR spectra of [**1**·HCl] (200 mM) at 193 K to prove both the protonation of the PO function and association, and to rule out the formation of a cube structure.

to the solution structures of the heavy chalcogenides? Once again, low temperature ^{15}N NMR spectroscopy provided clarity on the conditions in solution.

After cooling a 200 mM DCM solution of the ^{15}N-labeled HCl adduct [**1**·HCl] from 298 K to 193 K, the broad ^{1}H NMR signal at 7.74 ppm splits into two signal sets that can be assigned to a major species (maj) [$\delta(^{1}H) = 5.79$ and 11.41 ppm] and a minor species (min) [$\delta(^{1}H) = 5.10$ and 10.45 ppm] (Figure 5, bottom, left). The broad downfield-shifted signal of each set at 11.41 ppm and 10.45 ppm, respectively, can be clearly assigned to an O–H group, and the corresponding highfield-shifted doublets (5.79 ppm and 5.10 ppm, respectively) belong to an NH_2 group ($^{1}J_{H-N}$ of the major species: 80.8 Hz). In conjunction with the ^{1}H DOSY measurements, it can be assumed that the major species at 193 K is an aggregated, supramolecular HCl adduct, which is composed of a zigzag-like, hydrogen-bonded chain structure with OH and NH_2 groups involved, similar to the solid-state structure (see Figure 2), whereas the minor species has a lower degree of aggregation (it could even be a monomeric HCl adduct), and both species are in equilibrium. ^{31}P NMR spectroscopy at 193 K also points in the same direction (Figure 5, bottom, middle), as the chemical shifts of 74.3 ppm (major species) and 63.6 ppm (minor species) agree very well with the averaged ^{31}P NMR signals of the concentration-dependent ^{31}P NMR spectra at 298 K. This conclusion was ultimately confirmed by ^{15}N NMR spectroscopy of [**1**·HCl] (200 mM) at 193 K (Figure 5, bottom, right): As with compound **1** [triplet at $\delta(^{15}N) = 28.4$ ppm, $^{1}J_{N-H} = 73.0$ Hz], the ^{15}N NMR spectrum of [**1**·HCl] shows a slightly asymmetrical triplet at $\delta(^{15}N) = 34.7$ ppm, which is now slightly shifted downfield compared to **1**. The $^{1}J_{N-H}$ coupling constant (83.4 Hz) of [**1**·HCl] is also slightly increased compared to **1**. The multiplicity nicely corresponds to an NH_2 group. The formation of a cubic structure involving NH_3 subunits can therefore be ruled out with certainty.

Quantum chemical calculations at the theoretical level M062X/6−311+G(d,p)[28–30] using the polarizable continuum model (PCM)[31] (solvent: DCM) provided a profound understanding of the expression of different hydrogen-bonding modes (**Ch**–H···X versus **N**–H···X) of the oxygen analog compared to the sulfur analog on a thermochemical basis (Scheme 2). The Gibbs energies (ΔG) for binding an HCl molecule to an aminophosphine chalcogenide molecule (Ch = O, S) via the chalcogen or the amino function allowed an estimate of the intrinsic proton affinity in the presence of an anion that is capable of hydrogen-bonding, here Cl^{-}. The assumption of monomeric HCl molecules as the predominant species in DCM solution is well supported by MD simulations (for details, see the SI). In the case of a single molecule of the aminophosphine oxide, the binding of an HCl molecule to the oxygen function is a clearly exergonic process at −43 kJ mol^{-1}. Thus, the **O**–H···Cl hydrogen-bond

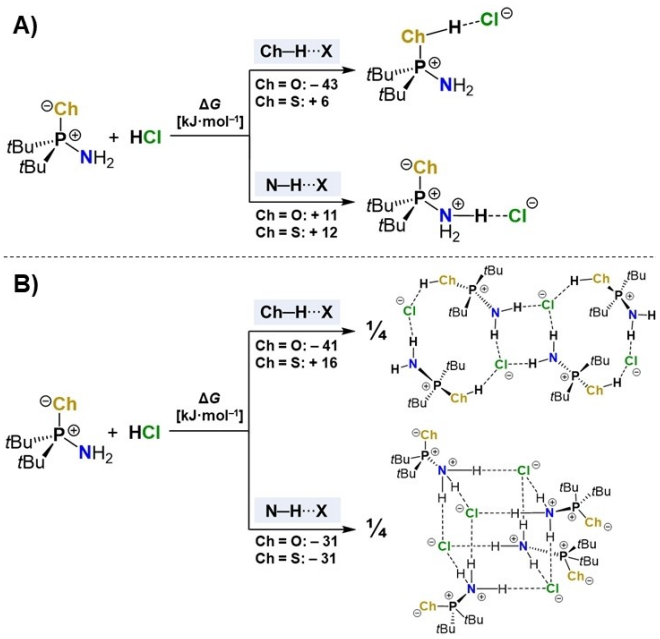

Scheme 2. Gibbs energies (ΔG) [kJ mol^{-1}] for the binding of HCl to aminophosphine chalcogenide molecules (Ch = O, S), calculated on the M062X/6−311 + G(d,p) level of theory (PCM, solvent: DCM).[28–31] Investigation of the intrinsic HCl binding affinity of the chalcogen and amino functions using monomeric systems (**A**). Estimation of the contribution of the hydrogen-bond network by considering plausible zigzag or cube shape superstructures of the hydrogen chloride adducts (**B**).

motif is energetically favored by 54 kJ mol^{-1} compared to the **N**–H···Cl motif (Scheme 2, **A**). In contrast, for the sulfide congener, both the expression of the **S**–H···Cl and the **N**–H···Cl binding modes are endergonic at 6 kJ mol^{-1} and 12 kJ mol^{-1}, respectively, assuming a system involving only one molecule of the aminophosphine chalcogenide (Scheme 2, **A**). The calculations excellently confirm the experimental finding regarding species $\mathbf{2}_{HCl}$ in DCM solution: After break-up of the cube structure, when the concentration decreases or the temperature increases, stable interactions can no longer be formed between monomeric phosphine **2** and HCl molecules, since the binding would represent an endergonic process. This fact is again supported and expressed by MD simulations, which show hardly any interactions between the neutral phosphine **2** and HCl molecules (for details, see the SI). For the very few hydrogen-bond interactions found in the MD simulation, the sulfur atom shows even better binding abilities than the NH_2 function, which is completely consistent with the results of the DFT calculations. Furthermore, the calculations allow for the important conclusion that, in contrast to the sulfur compound (**2**), an HCl molecule should actually bind to compound **1** even at very low concentrations, and this was indeed observed in our NMR investigation (see Figure 5).

To draw an even more precise picture, we also performed thermodynamic calculations considering the actual zigzag or cube shape of the HCl adducts to estimate the contribution of the entire hydrogen-bond network to the formation of just one very specific superstructure, depending on whether the oxygen or sulfur functionality is present (Scheme 2, **B**). These results show very clearly that it is in principle an energetically unfavorable option for the aminophosphine sulfide to involve the sulfur function in binding to an HCl molecule. The formation of a zigzag-like structure in which **S**–H···Cl···H–**N** structural motifs are present at the same time is a strongly endergonic process with $\Delta G = 16$ kJ mol^{-1} and can thus be ruled out in this case. Instead, the energy gain from the participation of all three hydrogen atoms of the NH_3 group in hydrogen-bonds to chloride acceptor atoms leads to an overcompensation for the energy that would have to be provided to bind just to a single chloride ion. The formation of a cubic assembly therefore becomes in principle favorable for both the sulfur and oxygen compounds, as shown by the Gibbs energies of −31 kJ mol^{-1} each. However, as clearly confirmed by the thermochemical calculations, for the oxygen derivative, the zigzag-like structure $[\mathbf{1}\cdot HCl]_n$, which is also the only structure that has been found in the solid-state so far, is significantly more favored (−41 kJ mol^{-1}) compared to a cubic association. In the case of the heavier congeners, it can be stated that the NH_2 group is only protonated if all three hydrogen atoms are available for hydrogen-bonds. The computational investigation also reveals a higher degree of flexibility of aminophosphine oxides in terms of their hydrogen-bond interaction pattern. The very similar energies suggest that both monomeric species with **O**–H···Cl (−43 kJ mol^{-1}) and aggregated structures with **O**–H···Cl···H–**N** bonding motifs (−41 kJ mol^{-1}) are equally likely to be formed in solution. The latter can be nicely deduced from the NMR spectra in solution, from which the formation of a cube structure for the oxygen case can definitely be ruled out (see Figure 5). In the case of the sulfur-based compound, we know that the cube shape is not only expressed in the solid-state, but also predominantly present in solution as the concentration increases or the temperature decreases. This is indeed the only way to create a real stable interaction between all heavier congeners and HCl molecules. Otherwise, the intermolecular contacts can just be considered as random encounters without stable hydrogen-bond interactions, as the MD simulations nicely confirm (see discussion above). These conclusions are also consistent with all experimental findings.

[Ch–H]$^+$ X$^-$ Versus [N–H]$^+$ X$^-$ Bonding

In a next step, we addressed the question of how the proton-binding affinity of aminophosphine chalcogenides changes when the coordinating anion, here Cl^-, is exchanged for a weakly coordinating anion (WCA), here $[B(C_6F_5)_4]^-$. For this purpose, compounds **1**, **2**, [(R_P)-**3**], and **4** were treated with Jutzi's acid $[H(OEt_2)_2]^+[B(C_6F_5)_4]^-$,[37] a synthetically useful and strong Brønsted acid that directly provides an anion incapable of forming hydrogen-bonds (Scheme 3).[38]

All protonated species could be isolated as ether-free solids. Both the sulfur- and selenium-based ion pairs $[\mathbf{2}H]^+[B(C_6F_5)_4]^-$ and $[\mathbf{4}H]^+[B(C_6F_5)_4]^-$ were also obtained in

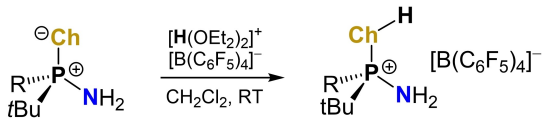

1: Ch = O, R = *t*Bu
2: Ch = S, R = *t*Bu
(R_P)-**3**: Ch = S, R = Cy
4: Ch = Se, R = *t*Bu

[**1**H]$^+$[B(C$_6$F$_5$)$_4$]$^-$, 85%
[**2**H]$^+$[B(C$_6$F$_5$)$_4$]$^-$, 87%
[(R_P)-**3**H]$^+$[B(C$_6$F$_5$)$_4$]$^-$, 82%
[**4**H]$^+$[B(C$_6$F$_5$)$_4$]$^-$, 74%

Scheme 3. Synthesis of protonated species of aminophosphine chalcogenides (Ch = O, S, Se) using Jutzi's acid[37] [H(OEt$_2$)$_2$]$^+$[B(C$_6$F$_5$)$_4$]$^-$ to study the effect of the weakly coordinating counteranion [B(C$_6$F$_5$)$_4$]$^-$ on the structure and dynamics of protonated species.

single-crystalline form and subjected to single-crystal X-ray structure analysis (Figure 6).[27] In the molecular structures of both compounds in the solid-state, it can be clearly seen that the protons bind exclusively to the chalcogen functions. No interactions between the cations can be detected. Instead, the cations are embedded in a shell of anions. The intermolecular interactions between cation and anion are striking. N–H···F interactions as well as direct N···F contacts can be found. While both the NH_2 and CH_3 groups are involved in directed contacts to the anion, the acidic Ch–H groups (Ch = S, Se) do not appear to be involved in anisotropic interactions (for details on crystal structure analysis, see the SI). Other bonding parameters of the cations in the crystal structures also indicate that the chalcogen function was protonated, such as a slight lengthening of the P–Ch and a slight shortening of the P–N bond compared to the parent compounds **2** and **4**.

The IR spectrum of compound [**2**H]$^+$[B(C$_6$F$_5$)$_4$]$^-$ in the solid-state provides further evidence for P–S protonation (Figure 7). The band at 2573 cm^{-1} can be clearly assigned to the S–H stretching vibration (Figure 7, top, red curve). The intriguing question, however, was whether the static bonding situation in the solid-state structure can actually be transferred to the structure in solution. IR spectroscopy of the ion pair [**2**H]$^+$[B(C$_6$F$_5$)$_4$]$^-$ in DCM solution also showed the characteristic S–H band at 2553 cm^{-1} (Figure 7, top, blue curve). The difference IR spectrum referred to the free aminophosphine sulfide **2** once again highlighted the reinforced N–H vibrations and the new S–H vibration of the

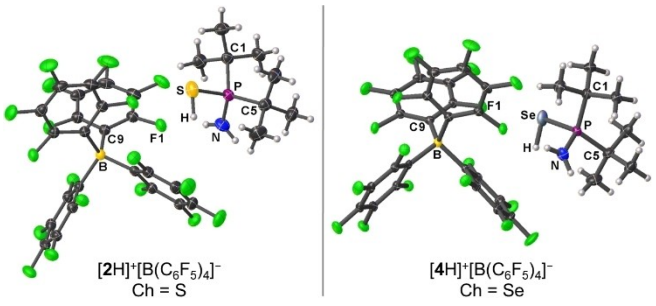

Figure 6. Molecular structures of the chalcogen-protonated sulfur and selenium derivatives [**2**H]$^+$[B(C$_6$F$_5$)$_4$]$^-$ and [**4**H]$^+$[B(C$_6$F$_5$)$_4$]$^-$ in the crystal (displacement ellipsoids are set at the 50% probability level).[27]

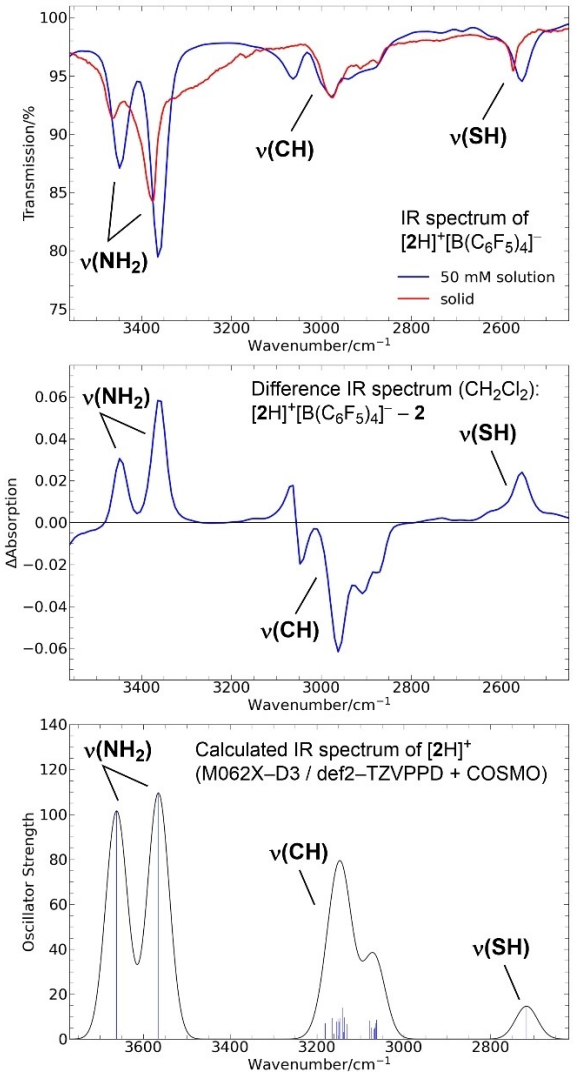

Figure 7. Evidence for P–S protonation. Top: Experimental IR spectra of ion pair [**2**H]$^+$[B(C$_6$F$_5$)$_4$]$^-$ in the solid-state (red curve) and in DCM solution (blue curve) clearly showing the SH stretching vibration. Middle: Difference IR spectrum in DCM solution ([**2**H]$^+$[B(C$_6$F$_5$)$_4$]$^-$ − **2**) highlighting the new SH vibration of the cation. Bottom: The calculated IR spectrum (no scaling factors applied) of cation [**2**H]$^+$ is in conformity with the experimental IR spectra.

cationic species [**2**H]$^+$ (Figure 7, middle). To further substantiate our conclusions, the experimental IR spectra are also excellently reflected in the calculated IR spectrum (Figure 7, bottom).

So, at this point, all data indicate that in the solid-state and in solution it is the chalcogen function that is protonated and not the amino group. It was therefore all the more surprising that the NH_2 and ChH groups belonging to the heavier congeners (Ch = S, Se) only gave one relatively sharp average signal in the ^{1}H NMR spectrum at 2.96 ppm or 2.94 ppm in case of the two sulfur-based compounds, and one signal at 2.48 ppm in case of the selenium compound. Although these signals are significantly downfield-shifted compared to the NH_2 signals of the parent compounds **2**, (R_P)-**3**, and **4**, they are still far from the ^{1}H NMR chemical

shift of an NH_3 unit that is involved in three hydrogen-bonds (see the discussion above). From studies on the protonated compound $[tBu_2(PSH)CH_2Si(H)tBu_2]^+[B(C_6F_5)_4]^-$ that does not have an NH_2 group, we know that the ^1H NMR chemical shift of the SH function of a protonated di-*tert*-butylphosphine sulfide moiety is 2.42 ppm, which is in fact in the same chemical shift region like the average PChH/PNH_2 ^1H NMR signal found in the protonated aminophosphine sulfides and the selenide (for details, see the spectroscopic data of compound $[\mathbf{5}H]^+[B(C_6F_5)_4]^-$ in the SI). However, since it is unlikely that the two ^1H NMR signals of the ChH and NH_2 functions coincidentally have the same chemical shift, we must assume that the protons undergo rapid exchange in solution.

To further support this hypothesis, ^{15}N NMR spectroscopy should be particularly informative since a collapse of the $^1J_{N-H}$ coupling would provide clear evidence of rapid proton exchange (Figure 8).[39] Indeed, in the ^1H-coupled ^{15}N NMR spectrum of compound $[\mathbf{2}H]^+[B(C_6F_5)_4]^-$, no $^1J_{N-H}$ coupling could be observed in DCM at either 298 K or 193 K. The spectrum even resembled the ^1H-decoupled $^{15}N\{^1H\}$ NMR spectrum of $[\mathbf{2}H]^+[B(C_6F_5)_4]^-$, whereas the $^1J_{N-P}$ coupling constant of 15.9 Hz as well as the chemical shift of $\delta(^{15}N) = 21.2$ ppm are clearly different from those of compound **2** ($\delta = 29.1$ ppm, $^1J_{N-P} = 22.2$ Hz). The missing ^{15}N–^1H splitting pattern in the ^1H-coupled ^{15}N NMR spectrum is strong evidence that rapid exchange occurs between the SH and NH_2 protons on the NMR time scale.

However, the situation is completely different with the oxygen derivative $[\mathbf{1}H]^+[B(C_6F_5)_4]^-$. Here, the exchange between the OH and NH_2 protons appears to be "frozen", since in this case, in contrast to the heavier analogs, the two functionalities can be clearly distinguished from each other in the ^1H NMR spectrum, with the signal at $\delta = 3.55$ ppm belonging to the PNH_2 function and the lowfield signal at $\delta = 6.04$ ppm belonging to the POH function.

In fact, this difference between the oxygen derivative and the heavier chalcogen compounds can be illustrated very well by DFT calculations [M062X/6−311+G(d,p); PCM solvent: DCM][28–31] of proton exchange reactions (Scheme 4). We calculated the Gibbs energy of the protonation of either the chalcogen or the amino function for both the oxygen and the sulfur derivative under the conditions of a protonation with Jutzi's acid $[H(OEt_2)_2]^+[B(C_6F_5)_4]^-$.[37] Therefore, $[H(OEt_2)_2]^+$ was chosen as the active proton source, which is known to be present under these conditions. For simplicity, any influence of the weakly coordinating anion was neglected in this model in order to shed light only on the intrinsic proton affinity. For both cases examined (Ch = O, S), protonation of the P–NH_2 function turned out to be thermodynamically indifferent. However, in the case of the oxygen compound, protonation of the PO function is energetically by far more favorable than the protonation of the NH_2 function ($\Delta G = -49$ kJ mol^{-1} versus -1 kJ mol^{-1}). This energy difference is so large that an OH/NH_2 proton exchange is thermodynamically severely restricted and hence two distinct signals can be observed in the ^1H NMR spectrum of compound $[\mathbf{1}H]^+[B(C_6F_5)_4]^-$. Furthermore, dimer formation between two cations in solution was clearly ruled out even in the case of smaller substituents (see the SI, Figure S123).

For the sulfur compound, the energy gap is much smaller (Scheme 4). Although the calculations show a preference for the protonation of the PS function, the protonation of the NH_2 group is only 13 kJ mol^{-1} higher in energy. It can be assumed that an equilibrium is quickly established between the two cationic forms in favor of the sulfur-protonated species. The intramolecular proton exchange is expected to occur with a low barrier, with tunneling effects likely playing an important role (Scheme 4, bottom).[40] Intermolecular proton exchange between two cations has also been

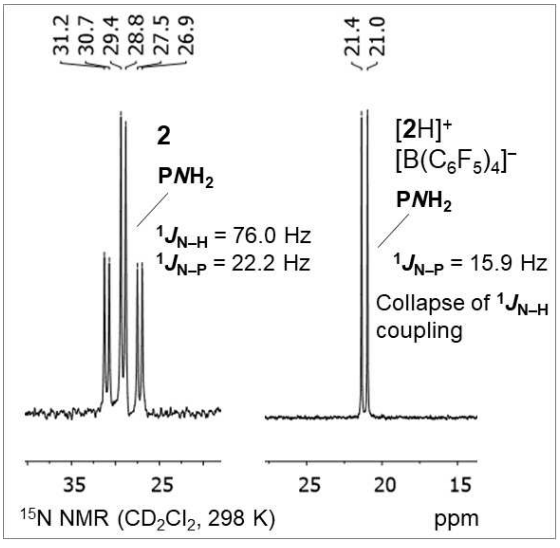

Figure 8. ^{15}N NMR spectrum of compound $[\mathbf{2}H]^+[B(C_6F_5)_4]^-$ (right) compared to that of compound **2** (left). The collapse of the $^1J_{N-H}$ coupling for the ion pair $[\mathbf{2}H]^+[B(C_6F_5)_4]^-$ in the ^1H-coupled ^{15}N NMR spectrum at 298 K (shown here) and even at 193 K provides clear evidence for rapid proton exchange.

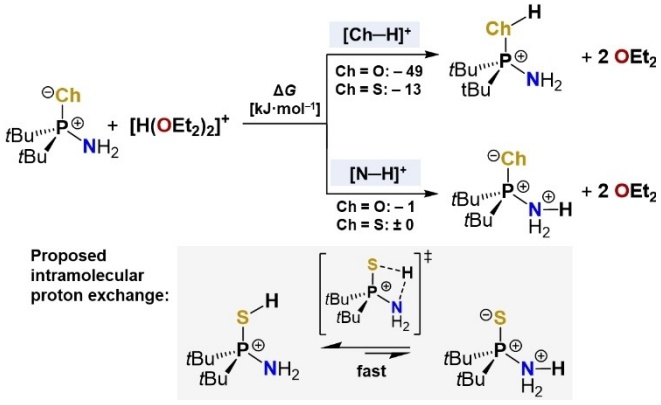

Scheme 4. Gibbs energies (ΔG) [kJ mol^{-1}] for the protonation of either the chalcogen or the amino function of aminophosphine chalcogenide molecules (Ch = O, S), calculated on the M062X/6−311+G(d,p) level of theory (PCM, solvent: DCM),[28–31] to study the intrinsic proton affinity in the absence of coordinating counterions (top). Proposed intramolecular mechanism of proton-hopping (bottom) supported by ^{15}N NMR spectroscopy.

considered but seems unlikely given the high energy ($\Delta G =$ 71 kJ mol^{-1}) required for dimer formation consisting of two cations (for details, see the SI, Figure S123).

Last but not least, the ^{77}Se nucleus, in particular the ^{77}Se NMR chemical shifts and the $^{1}J_{Se-P}$ coupling constants, can also serve as an effective NMR probe to further confirm the protonation of the chalcogenide function in the heavier congeners. Only when the selenium atom is directly involved in an interaction with the proton, the $^{1}J_{Se-P}$ coupling constant decreases significantly by almost half from 726.6 Hz in **4** to 406.3 Hz in $[\mathbf{4}H]^+[B(C_6F_5)_4]^-$. This is accompanied by a dramatic large downfield shift from $\delta(^{77}Se) = -350.8$ ppm to −43.4 ppm. The effects on the ^{77}Se NMR spectroscopic parameters in the case of a direct interaction of the selenium atom in phosphine selenides with Lewis acids have recently been discussed in detail.[41]

Conclusion

Combining spectroscopic (IR, ^{1}H DOSY, ^{15}N NMR), quantum chemistry-based methods, MD simulations, and crystallographic analyses, our work provided in-depth insights into the structure and dynamics of proton-binding and the hydrogen-bond switching ability of aminophosphine chalcogenides as the fundamental basis of supramolecular self-assembly processes.

Expression of structural motif **I** (**Ch**–**H**···**X**, see Figure 1, D) in the presence of anions capable of coordination, here chloride, is only observed in the case of aminophosphine oxide **1**. Protonation of the P–O function in the form of a hydrogen-bonded zigzag-like **O**–H···Cl···H–**N** arrangement wins energetically over a cube assembly. In the heavier congeners **2**, (R_P)-**3**, and **4** (Ch = S, Se), protonation of the P–Ch function never occurs in the presence of coordinating anions. The protonation of the P–NH_2 function, according to the structural motif **II** (**N**–**H**···**Cl**), occurs only if all three **N**–H bonds can actually be involved in hydrogen-bonds. Here, MD simulations provided first insight into the self-organization process of aminophosphate-analog species toward a cube arrangement. The findings at the lower concentration limit appear particularly interesting, as this is also where a main difference lies between the heavier congeners and the oxygen derivative. In fact, it was shown that the existence of a stable **O**–H···Cl bond is maintained even at very low concentrations, and this is in sharp contrast to the heavier chalcogenides. The crystal structures also reflect a delicate balance between different hydrogen-bond interaction pattern. Given the key role that aminophosphates play in phosphorylation mechanisms of prebiotically relevant molecules and in scenarios for the emergence of homochirality,[19,20,21d] our study reveals a significant advantage of the H_2N–P^+–O^- compared to the H_2N–P^+–S^- functional pattern in terms of the flexibility of the lighter congener to involve both NH_2 and OH groups in hydrogen-bonding and self-assembly processes. Another advantage of the H_2N–P^+–O^- functionality is expressed in the easier formation of stable and rigid interactions with protic compounds at different concentrations.

In the case of weakly coordinating anions (WCAs) as counterions, here $[B(C_6F_5)_4]^-$, there is a clear intrinsic preference for protonation of the P–Ch function over the NH_2 function for all chalcogenide derivatives according to the structural motif **III** (**[Ch–H]$^+$ X$^-$**), regardless of Pearson's principle of hard and soft acids and bases (HSAB).[42] Nevertheless, the dynamic behavior of the protonated heavier chalcogenides in solution differs significantly from the oxygen compound. For the protonated aminophosphine sulfide $[\mathbf{2}H]^+[B(C_6F_5)_4]^-$, the collapse of the $^{1}J_{N-H}$ coupling indicates a fast equilibrium between the two protonated forms **III** (**[S–H]$^+$ WCA$^-$**) and **IV** (**[N–H]$^+$ WCA$^-$**) in the form of a dynamic, intramolecular process of rapid proton-hopping between the chalcogen atom and the amino function. This second part of our investigation may have significant consequences for a new design of bifunctional organocatalysts, as the replacement of the proton by an organic residue can pave a new route to combined chalcogen- and hydrogen-bonding catalysis.

The significance of this study extends to many areas of catalysis, be it the field of hydrogen-bonding, ion-pairing, or chalcogen-bonding catalysis. Viewed in the light of prebiotic chemistry, our results on aminophosphate-analog systems also provide important new insights into the behavior of fundamental protonated species that play a crucial role as intermediates in phosphorylation processes and in scenarios for the emergence of homochirality. Work is currently being done on the behavior of these species in aqueous solution.

Supporting Information

The authors have cited additional references within the Supporting Information.[43–72]

Acknowledgements

This project was financed by the Deutsche Forschungsgemeinschaft (DFG, German Research Foundation) through the Research Training Group "Ion Pair Effects in Molecular Reactivity" (RTG 2620, Project 426795949). Further support was provided by the Elite Network of Bavaria (ENB) and the Bavarian State Ministry of Science and the Arts (StMWK, Project N-LW-NW-2016-366). M.K. thanks the Fonds der Chemischen Industrie (FCI) for a Kekulé fellowship. Open Access funding enabled and organized by Projekt DEAL.

Conflict of Interest

The authors declare no conflict of interest.

Data Availability Statement

The data that support the findings of this study are available in the supplementary material of this article.

Keywords: Hydrogen bonds · Molecular dynamics · NMR spectroscopy · Protonation · Self-assembly

[1] a) G. A. Jeffrey, W. Saenger, *Hydrogen Bonding in Biological Structures*, Springer-Verlag, New York, USA, **1991**; b) L. E. Orgel, *Nature* **1992**, *358*, 203–209; c) J.-M. Lehn, *Science* **1993**, *260*, 1762–1763; d) T. Steiner, *Angew. Chem. Int. Ed.* **2002**, *41*, 48–76; e) J.-M. Lehn, *Supramolecular Chemistry: Concepts and Perspectives*, Wiley-VCH, Weinheim, Germany, **2006**; f) D. A. Uhlenheuer, K. Petkau, L. Brunsveld, *Chem. Soc. Rev.* **2010**, *39*, 2817–2826; g) M. J. Webber, E. A. Appel, E. W. Meijer, R. Langer, *Nat. Mater.* **2016**, *15*, 13–26; h) Y. Tu, F. Peng, A. Adawy, Y. Men, L. K. E. A. Abdelmohsen, D. A. Wilson, *Chem. Rev.* **2016**, *116*, 2023–2078; i) M. P. Hendricks, K. Sato, L. C. Palmer, S. I. Stupp, *Acc. Chem. Res.* **2017**, *50*, 2440–2448.

[2] a) M. S. Taylor, E. N. Jacobsen, *Angew. Chem. Int. Ed.* **2006**, *45*, 1520–1543; b) A. G. Doyle, E. N. Jacobsen, *Chem. Rev.* **2007**, *107*, 5713–5743; c) U. Gellrich, W. Seiche, M. Keller, B. Breit, *Angew. Chem. Int. Ed.* **2012**, *51*, 11033–11038; d) K. M. Wenz, G. Leonhardt-Lutterbeck, B. Breit, *Angew. Chem. Int. Ed.* **2018**, *57*, 5100–5104.

[3] a) N. D. Shapiro, V. Rauniyar, G. L. Hamilton, J. Wu, F. D. Toste, *Nature* **2011**, *470*, 245–249; b) D. Parmar, E. Sugiono, S. Raja, M. Rueping, *Chem. Rev.* **2014**, *114*, 9047–9153; c) I. Harden, F. Neese, G. Bistoni, *Chem. Sci.* **2023**, *14*, 10580–10590.

[4] a) S. E. Denmark, S. K. Ghosh, *Angew. Chem. Int. Ed.* **2001**, *40*, 4759–4762; b) S. E. Denmark, J. Fu, *Chem. Rev.* **2003**, *103*, 2763–2793; c) M. Rueping, B. J. Nachtsheim, S. A. Moreth, M. Bolte, *Angew. Chem. Int. Ed.* **2008**, *47*, 593–596; d) S. Vellalath, I. Čorić, B. List, *Angew. Chem. Int. Ed.* **2010**, *49*, 9749–9752; e) I. Čorić, B. List, *Nature* **2012**, *483*, 315–319; f) J. H. Kim, I. Čorić, S. Vellalath, B. List, *Angew. Chem. Int. Ed.* **2013**, *52*, 4474–4477.

[5] a) M. Fleischmann, D. Drettwan, E. Sugiono, M. Rueping, R. M. Gschwind, *Angew. Chem. Int. Ed.* **2011**, *50*, 6364–6369; b) J. Greindl, J. Hioe, N. Sorgenfrei, F. Morana, R. M. Gschwind, *J. Am. Chem. Soc.* **2016**, *138*, 15965–15971; c) M. Melikian, J. Gramüller, J. Hioe, J. Greindl, R. M. Gschwind, *Chem. Sci.* **2019**, *10*, 5226–5234; d) K. Rothermel, M. Melikian, J. Hioe, J. Greindl, J. Gramüller, M. Žabka, N. Sorgenfrei, T. Hausler, F. Morana, R. M. Gschwind, *Chem. Sci.* **2019**, *10*, 10025–10034; e) N. Lokesh, J. Hioe, J. Gramüller, R. M. Gschwind, *J. Am. Chem. Soc.* **2019**, *141*, 16398–16407; f) D. Jansen, J. Gramüller, F. Niemeyer, T. Schaller, M. C. Letzel, S. Grimme, H. Zhu, R. M. Gschwind, J. Niemeyer, *Chem. Sci.* **2020**, *11*, 4381–4390; g) N. Berg, S. Bergwinkl, P. Nuernberger, D. Horinek, R. M. Gschwind, *J. Am. Chem. Soc.* **2021**, *143*, 724–735; h) J. Eder, A. S. Antonov, E. Y. Tupikina, R. M. Gschwind, *Chem. Eur. J.* **2024**, *30*, e202401793.

[6] a) M. Hayashi, Y. Hashimoto, Y. Yamamoto, J. Usuki, K. Saigo, *Angew. Chem. Int. Ed.* **2000**, *39*, 631–633; b) E. Ichikawa, M. Suzuki, K. Yabu, M. Albert, M. Kanai, M. Shibasaki, *J. Am. Chem. Soc.* **2004**, *126*, 11808–11809; c) S.-i. Aizawa, A. Majumder, Y. Yokoyama, M. Tamai, D. Maeda, A. Kitamura, *Organometallics* **2009**, *28*, 6067–6072.

[7] a) L. B. Balázs, J. B. Khalikuzzaman, Y. Li, D. Csókás, S. A. Pullarkat, P.-H. Leung, *Chem. Commun.* **2019**, *55*, 10936–10939; b) W.-J. Yue, J.-Z. Xiao, S. Zhang, L. Yin, *Angew. Chem. Int. Ed.* **2020**, *59*, 7057–7062.

[8] Review: M. Hayashi, *Chem. Lett.* **2021**, *50*, 1–6.

[9] a) S. Furukawa, Y. Suda, J. Kobayashi, T. Kawashima, T. Tada, S. Fujii, M. Kiguchi, M. Saito, *J. Am. Chem. Soc.* **2017**, *139*, 5787–5792; b) S. Fujii, M. Iwane, S. Furukawa, T. Tada, T. Nishino, M. Saito, M. Kiguchi, *J. Phys. Chem. C* **2020**, *124*, 9261–9268; c) E. Martín-Encinas, V. Conejo-Rodríguez, J. A. Miguel, J. M. Martínez-Ilarduya, G. Rubiales, B. R. Knudsen, F. Palacios, C. Alonso, *Dalton Trans.* **2020**, *49*, 7852–7861.

[10] a) T. Cantat, X. Jacques, L. Ricard, X. F. Le Goff, N. Mézailles, P. Le Floch, *Angew. Chem. Int. Ed.* **2007**, *46*, 5947–5950; b) P. Schröter, V. H. Gessner, *Chem. Eur. J.* **2012**, *18*, 11223–11227; c) H. Heuclin, S. Y.-F. Ho, X. F. Le Goff, C.-W. So, N. Mézailles, *J. Am. Chem. Soc.* **2013**, *135*, 8774–8777; d) S. Molitor, V. H. Gessner, *Angew. Chem. Int. Ed.* **2016**, *55*, 7712–7716.

[11] a) W. Wang, H. Zhu, L. Feng, Q. Yu, J. Hao, R. Zhu, Y. Wang, *J. Am. Chem. Soc.* **2020**, *142*, 3117–3124; b) X. Kong, P.-P. Zhou, Y. Wang, *Angew. Chem. Int. Ed.* **2021**, *60*, 9395–9400; c) X. Yuan, Y. Wang, *Angew. Chem. Int. Ed.* **2022**, *61*, e202203671; d) Z. Zhao, Y. Pang, Z. Zhao, P.-P. Zhou, Y. Wang, *Nat. Commun.* **2023**, *14*, 6347; e) Z. Zhao, Y. Wang, *Acc. Chem. Res.* **2023**, *56*, 608–621; f) W. Ma, J.-L. Kirchhoff, C. Strohmann, B. Grabe, C. C. J. Loh, *J. Am. Chem. Soc.* **2023**, *145*, 26611–26622; g) H. Guo, J.-L. Kirchhoff, C. Strohmann, B. Grabe, C. C. J. Loh, *Angew. Chem. Int. Ed.* **2024**, *63*, e202316667; h) W. Ma, A. Schmidt, C. Strohmann, C. C. J. Loh, *Angew. Chem. Int. Ed.* **2024**, *63*, e202405706.

[12] a) M. A. Pasek, J. P. Dworkin, D. S. Lauretta, *Geochim. Cosmochim. Acta* **2007**, *71*, 1721–1736; b) D. E. Bryant, D. Greenfield, R. D. Walshaw, B. R. G. Johnson, B. Herschy, C. Smith, M. A. Pasek, R. Telford, I. Scowen, T. Munshi, H. G. M. Edwards, C. R. Cousins, I. A. Crawford, T. P. Kee, *Geochim. Cosmochim. Acta* **2013**, *109*, 90–112; c) A. J. Wagner, D. G. Blackmond, *ACS Cent. Sci.* **2016**, *2*, 775–777; d) M. A. Pasek, M. Gull, B. Herschy, *Chem. Geol.* **2017**, *475*, 149–170; e) C. Fernández-García, A. J. Coggins, M. W. Powner, *Life* **2017**, *7*, 31; f) N. Kitadai, S. Maruyama, *Geosci. Front.* **2018**, *9*, 1117–1153; g) Z. Liu, J.-C. Rossi, R. Pascal, *Life* **2019**, *9*, 26; h) M. A. Pasek, *Chem. Rev.* **2020**, *120*, 4690–4706; i) M. Yadav, R. Kumar, R. Krishnamurthy, *Chem. Rev.* **2020**, *120*, 4766–4805; j) A. Franco, J. A. L. da Silva, *Angew. Chem. Int. Ed.* **2021**, *60*, 10458–10468; k) C. R. Walton, S. Ewens, J. D. Coates, R. E. Blake, N. J. Planavsky, C. Reinhard, P. Ju, J. Hao, M. A. Pasek, *Nat. Geosci.* **2023**, *16*, 399–409.

[13] a) R. Krishnamurthy, S. Guntha, A. Eschenmoser, *Angew. Chem. Int. Ed.* **2000**, *39*, 2281–2285; b) M. Karki, C. Gibard, S. Bhowmik, R. Krishnamurthy, *Life* **2017**, *7*, 32; c) C. Gibard, S. Bhowmik, M. Karki, E.-K. Kim, R. Krishnamurthy, *Nat. Chem.* **2018**, *10*, 212–217; d) C. Gibard, I. B. Gorrell, E. I. Jiménez, T. P. Kee, M. A. Pasek, R. Krishnamurthy, *Angew. Chem. Int. Ed.* **2019**, *58*, 8151–8155.

[14] D. J. Ritson, J. Xu, J. D. Sutherland, *Synlett* **2017**, *28*, 64–67.

[15] D. J. Ritson, S. J. Mojzsis, J. D. Sutherland, *Nat. Geosci.* **2020**, *13*, 344–348.

[16] R. M. Gschwind, M. Armbrüster, I. Z. Zubrzycki, *J. Am. Chem. Soc.* **2004**, *126*, 10228–10229.

[17] A. Berkessel, H. Gröger, *Asymmetric Organocatalysis: From Biomimetic Concepts to Applications in Asymmetric Synthesis*, Wiley-VCH, Weinheim, **2005**.

[18] a) J. Gramüller, P. Dullinger, D. Horinek, R. M. Gschwind, *Chem. Sci.* **2022**, *13*, 14366–14372; b) M. Franta, J. Gramüller, P. Dullinger, S. Kaltenberger, D. Horinek, R. M. Gschwind, *Angew. Chem. Int. Ed.* **2023**, *62*, e202301183.

[19] a) M. W. Powner, B. Gerland, J. D. Sutherland, *Nature* **2009**, *459*, 239–242; b) A. J. Coggins, M. W. Powner, *Nat. Chem.* **2017**, *9*, 310–317; c) H. A. Cruz, E. I. Jiménez, R. Krishnamurthy, *J. Am. Chem. Soc.* **2023**, *145*, 23781–23793.

[20] a) A. W. Garrison, C. E. Boozer, *J. Am. Chem. Soc.* **1968**, *90*, 3486–3494; b) T. Koizumi, P. Haake, *J. Am. Chem. Soc.* **1973**, *95*, 8073–8079; c) T. A. Modro, W. G. Liauw, M. R. Peterson, I. G. Csizmadiac, *J. Chem. Soc. Perkin Trans. 2* **1979**, 1432–1436; d) M. P. Gamcsik, S. M. Ludeman, E. M. Shulman-

Roskes, I. J. McLennan, M. E. Colvin, O. M. Colvin, *J. Med. Chem.* **1993**, *36*, 3636–3645.
[21] a) G. R. J. Thatcher, A. S. Campbell, *J. Org. Chem.* **1993**, *58*, 2272–2281; b) A. J. Kirby, F. Nome, *Acc. Chem. Res.* **2015**, *48*, 1806–1814; c) K. W. Knouse, D. T. Flood, J. C. Vantourout, M. A. Schmidt, I. M. Mcdonald, M. D. Eastgate, P. S. Baran, *ACS Cent. Sci.* **2021**, *7*, 1473–1485; d) V. Dašková, Jeffrey Buter, A. K. Schoonen, M. Lutz, F. de Vries, B. L. Feringa, *Angew. Chem. Int. Ed.* **2021**, *60*, 11120–11126; e) V. Dašková, D. Padín, B. L. Feringa, *J. Am. Chem. Soc.* **2022**, *144*, 23603–23613.
[22] a) J. L. Bada, *Nature* **1995**, *374*, 594–595; b) B. L. Feringa, R. A. van Delden, *Angew. Chem. Int. Ed.* **1999**, *38*, 3418–3438; c) A. R. A. Palmans, E. W. Meijer, *Angew. Chem. Int. Ed.* **2007**, *46*, 8948–8968; d) I. Weissbuch, M. Lahav, *Chem. Rev.* **2011**, *111*, 3236–3267; e) D. G. Blackmond, *Chem. Rev.* **2020**, *120*, 4831–4847.
[23] Reviews: a) A. Cabré, A. Riera, X. Verdaguer, *Acc. Chem. Res.* **2020**, *53*, 676–689; b) T. Huber, J. O. Bauer, *Chem. Eur. J.* **2024**, *30*, e202303760.
[24] a) M. Bonsignore, M. Benaglia, F. Cozzi, A. Genoni, S. Rossi, L. Raimondi, *Tetrahedron* **2012**, *68*, 8251–8255; b) Z. S. Han, L. Zhang, Y. Xu, J. D. Sieber, M. A. Marsini, Z. Li, J. T. Reeves, K. R. Fandrick, N. D. Patel, J.-N. Desrosiers, B. Qu, A. Chen, D. M. Rudzinski, L. P. Samankumara, S. Ma, N. Grinberg, F. Roschangar, N. K. Yee, G. Wang, J. J. Song, C. H. Senanayake, *Angew. Chem. Int. Ed.* **2015**, *54*, 5474–5477; c) W. Zhao, P. K. Yan, A. T. Radosevich, *J. Am. Chem. Soc.* **2015**, *137*, 616–619; d) X.-L. Qin, A. Li, F.-S. Han, *J. Am. Chem. Soc.* **2021**, *143*, 2994–3002.
[25] a) I. G. Shenderovich, P. M. Tolstoy, N. S. Golubev, S. N. Smirnov, G. S. Denisov, H.-H. Limbach, *J. Am. Chem. Soc.* **2003**, *125*, 11710–11720; b) S. B. Lesnichin, P. M. Tolstoy, H.-H. Limbach, I. G. Shenderovich, *Phys. Chem. Chem. Phys.* **2010**, *12*, 10373–10379.
[26] T. Huber, N. A. Espinosa-Jalapa, J. O. Bauer, *Chem. Eur. J.* **2022**, *28*, e202202608.
[27] Deposition numbers CCDC 2358975 (for **2**), CCDC 2358976 (for **4**), CCDC 2358977 (for $[\mathbf{2H}]^+[B(C_6F_5)_4]^-$), CCDC 2358978 (for $[\mathbf{4}\cdot HCl]_4$), CCDC 2358979 (for $[\mathbf{2}\cdot HCl]_4$), CCDC 2358980 (for $[\mathbf{4H}]^+[B(C_6F_5)_4]^-$), CCDC 2358981 (for $[\mathbf{5H}]^+[B(C_6F_5)_4]^-$), CCDC 2358982 (for [**1**·HCl]), CCDC 2358983 (for $[(R_P)$-$\mathbf{3}\cdot HCl]_4$), CCDC 2411478 (for (*rac*)-**3**), and CCDC 2411479 (for $[(rac)$-$\mathbf{3}\cdot HCl]_4$) contain the supplementary crystallographic data for this paper. These data are provided free of charge by the joint Cambridge Crystallographic Data Centre and Fachinformationszentrum Karlsruhe Access Structures service.
[28] Y. Zhao, D. G. Truhlar, *Theor. Chem. Acc.* **2008**, *120*, 215–241.
[29] a) R. Krishnan, J. S. Binkley, R. Seeger, J. A. Pople, *J. Chem. Phys.* **1980**, *72*, 650–654; b) A. D. McLean, G. S. Chandler, *J. Chem. Phys.* **1980**, *72*, 5639–5648; c) T. Clark, J. Chandrasekhar, G. W. Spitznagel, P. v. R. Schleyer, *J. Comput. Chem.* **1983**, *4*, 294–301.
[30] M. J. Frisch, G. W. Trucks, H. B. Schlegel, G. E. Scuseria, M. A. Robb, J. R. Cheeseman, G. Scalmani, V. Barone, B. Mennucci, G. A. Petersson, H. Nakatsuji, M. Caricato, X. Li, H. P. Hratchian, A. F. Izmaylov, J. Bloino, G. Zheng, J. L. Sonnenberg, M. Hada, M. Ehara, K. Toyota, R. Fukuda, J. Hasegawa, M. Ishida, T. Nakajima, Y. Honda, O. Kitao, H. Nakai, T. Vreven, J. A. Montgomery Jr., J. E. Peralta, F. Ogliaro, M. Bearpark, J. J. Heyd, E. Brothers, K. N. Kudin, V. N. Staroverov, T. Keith, R. Kobayashi, J. Normand, K. Raghavachari, A. Rendell, J. C. Burant, S. S. Iyengar, J. Tomasi, M. Cossi, N. Rega, J. M. Millam, M. Klene, J. E. Knox, J. B. Cross, V. Bakken, C. Adamo, J. Jaramillo, R. Gomperts, R. E. Stratmann, O. Yazyev, A. J. Austin, R. Cammi, C. Pomelli, J. W. Ochterski, R. L. Martin, K. Morokuma, V. G. Zakrzewski, G. A. Voth, P. Salvador, J. J. Dannenberg, S. Dapprich, A. D. Daniels, O. Farkas, J. B. Foresman, J. V. Ortiz, J. Cioslowski, D. J. Fox, *Gaussian 09*. Revision E.01; Gaussian, Inc.: Wallingford, CT, USA, **2013**.
[31] J. Tomasi, B. Mennucci, R. Cammi, *Chem. Rev.* **2005**, *105*, 2999–3093.
[32] a) W. B. Blanton, S. W. Gordon-Wylie, G. R. Clark, K. D. Jordan, J. T. Wood, U. Geiser, T. J. Collins, *J. Am. Chem. Soc.* **1999**, *121*, 3551–3552; b) T. A. Beu, U. Buck, *J. Chem. Phys.* **2001**, *114*, 7848–7852; c) S. D. Belair, J. S. Francisco, *Phys. Rev. A* **2003**, *67*, 063206; d) B. F. Abrahams, M. G. Haywood, T. A. Hudson, R. Robson, *Angew. Chem. Int. Ed.* **2004**, *43*, 6157–6160; e) B. F. Abrahams, M. G. Haywood, R. Robson, *J. Am. Chem. Soc.* **2005**, *127*, 816–817; f) S. D. Belair, J. S. Francisco, S. J. Singer, *Phys. Rev. A* **2005**, *71*, 013204.
[33] a) C. J. Gruenloh, J. R. Carney, C. A. Arrington, T. S. Zwier, S. Y. Fredericks, K. D. Jordan, *Science* **1997**, *276*, 1678–1681; b) L. R. MacGillivray, J. L. Atwood, *Nature* **1997**, *389*, 469–472; c) G. Li, Y.-Y. Zhang, Q. Li, C. Wang, Y. Yu, B. Zhang, H.-S. Hu, W. Zhang, D. Dai, G. Wu, D. H. Zhang, J. Li, X. Yang, L. Jiang, *Nat. Commun.* **2020**, *11*, 5449.
[34] a) J. Büchler, C. Maichle-Mössmer, K.-A. Kovar, *Z. Naturforsch. B* **2000**, *55*, 1124–1130; b) A. D. Bond, E. L. Doyle, *Chem. Commun.* **2003**, 2324–2325; c) K. Sada, T. Watanabe, J. Miyamoto, T. Fukuda, N. Tohnai, M. Miyata, T. Kitayama, K. Maehara, K. Ute, *Chem. Lett.* **2004**, *33*, 160–161; d) B. Becker, K. Baranowska, J. Chojnacki, W. Wojnowski, *Chem. Commun.* **2004**, 620–621; e) A. D. Bond, *Cryst. Growth Des.* **2005**, *5*, 755–771; f) A. D. Bond, *Coord. Chem. Rev.* **2005**, *249*, 2035–2055; g) A. D. Bond, W. H. Jørgensen, J. M. Pløger, *Chem. Commun.* **2007**, 3273–3275; h) N. Tohnai, Y. Mizobe, M. Doi, S. Sukata, T. Hinoue, T. Yuge, I. Hisaki, Y. Matsukawa, M. Miyata, *Angew. Chem. Int. Ed.* **2007**, *46*, 2220–2223; i) T. Yuge, N. Kai, I. Hisaki, M. Miyata, N. Tohnai, *Chem. Lett.* **2007**, *36*, 1390–1391; j) T. Yuge, N. Tohnai, T. Fukuda, I. Hisaki, M. Miyata, *Chem. Eur. J.* **2007**, *13*, 4163–4168; k) T. Yuge, I. Hisaki, M. Miyata, N. Tohnai, *CrystEngComm* **2008**, *10*, 263–266; l) A. Yamamoto, T. Hamada, I. Hisaki, M. Miyata, N. Tohnai, *Angew. Chem. Int. Ed.* **2013**, *52*, 1709–1712; m) T. Sasaki, Y. Ida, T. Yuge, A. Yamamoto, I. Hisaki, N. Tohnai, M. Miyata, *Cryst. Growth Des.* **2015**, *15*, 658–665.
[35] a) Y. Cohen, L. Avram, L. Frish, *Angew. Chem. Int. Ed.* **2005**, *44*, 520–554; b) H. Zhang, R. Kerssebaum, R. M. Gschwind, *Magn. Reson. Chem.* **2009**, *47*, 568–572; c) K. Schober, E. Hartmann, H. Zhang, R. M. Gschwind, *Angew. Chem. Int. Ed.* **2010**, *49*, 2794–2797; d) N. A. Espinosa-Jalapa, N. Berg, M. Seidl, I. G. Shenderovich, R. M. Gschwind, J. O. Bauer, *Chem. Commun.* **2020**, *56*, 13335–13338; e) N. Geue, R. E. P. Winpenny, P. E. Barran, *Chem. Soc. Rev.* **2022**, *51*, 8–27.
[36] a) G. Binsch, J. B. Lambert, B. W. Roberts, J. D. Roberts, *J. Am. Chem. Soc.* **1964**, *86*, 5564–5570; b) J. Müller, *Z. Naturforsch. B* **1978**, *33*, 993–996; c) W. von Philipsborn, R. Müller, *Angew. Chem. Int. Ed.* **1986**, *25*, 383–413.
[37] P. Jutzi, C. Müller, A. Stammler, H.-G. Stammler, *Organometallics* **2000**, *19*, 1442–1444.
[38] a) N. Fontana, N. A. Espinosa-Jalapa, M. Seidl, J. O. Bauer, *Chem. Eur. J.* **2021**, *27*, 2649–2653; b) N. Fontana, N. A. Espinosa-Jalapa, M. Seidl, J. O. Bauer, *Chem. Commun.* **2022**, *58*, 2144–2147.
[39] J. Schraml, P. Cigler, *Magn. Reson. Chem.* **2008**, *46*, 748–755.
[40] a) N. Shida, J. Almlöf, P. F. Barbara, *J. Phys. Chem.* **1991**, *95*, 10457–10464; b) K. Umesaki, K. Odai, *J. Phys. Chem. A* **2023**, *127*, 1046–1052.
[41] a) A. Falk, J. O. Bauer, *Inorg. Chem.* **2022**, *61*, 15576–15588; b) N. Fontana, J. O. Bauer, *ChemistrySelect* **2023**, *8*, e202301373.

[42] a) R. G. Pearson, *J. Am. Chem. Soc.* **1963**, *85*, 3533–3539; b) R. G. Pearson, J. Songstad, *J. Am. Chem. Soc.* **1967**, *89*, 1827–1836; c) R. G. Pearson, *J. Chem. Educ.* **1968**, *45*, 581–587; d) R. G. Pearson, *J. Chem. Educ.* **1968**, *45*, 643–648; e) T.-L. Ho, *Chem. Rev.* **1975**, *75*, 1–20.
[43] S. F. Rach, E. Herdtweck, F. E. Kühn, *J. Organomet. Chem.* **2011**, *696*, 1817–1823.
[44] M. Köster, A. Kreher, C. von Hänisch, *Dalton Trans.* **2018**, *47*, 7875–7878.
[45] M. J. P. Hargar, M. A. Stephen, *J. Chem. Soc. Perkin Trans. 1* **1980**, 705–711.
[46] a) A. P. Stewart, S. Trippett, *J. Chem. Soc. C* **1970**, 1263–1266; b) W. Kuchen, G. Hägele, *Chem. Ber.* **1970**, *103*, 2114–2121.
[47] A. Jerschow, N. Müller, *J. Magn. Reson.* **1997**, *125*, 372–375.
[48] A. Macchioni, G. Ciancaleoni, C. Zuccaccia, D. Zuccaccia, *Chem. Soc. Rev.* **2008**, *37*, 479–489.
[49] H.-C. Chen, S.-H. Chen, *J. Phys. Chem.* **1984**, *88*, 5118–5121.
[50] D. Ben-Amotz, K. G. Willis, *J. Phys. Chem.* **1993**, *97*, 7736–7742.
[51] D. Zuccaccia, A. Macchioni, *Organometallics* **2005**, *24*, 3476–3486.
[52] Rigaku Oxford Diffraction, CrysAlisPro Software System, **2023**.
[53] O. V. Dolomanov, L. J. Bourhis, R. J. Gildea, J. A. K. Howard, H. Puschmann, *J. Appl. Crystallogr.* **2009**, *42*, 339–341.
[54] G. M. Sheldrick, *Acta Crystallogr. Sect. A* **2015**, *71*, 3–8.
[55] G. M. Sheldrick, *Acta Crystallogr. Sect. C* **2015**, *71*, 3–8.
[56] a) M. A. Spackman, J. J. McKinnon, *CrystEngComm* **2002**, *4*, 378–392; b) M. A. Spackman, D. Jayatilaka, *CrystEngComm* **2009**, *11*, 19–32.
[57] a) M. J. Turner, J. J. McKinnon, S. K. Wolff, D. J. Grimwood, P. R. Spackman, D. Jayatilaka, M. A. Spackman, *CrystalExplorer17*, University of Western Australia, Perth (Australia), **2017**; b) P. R. Spackman, M. J. Turner, J. J. McKinnon, S. K. Wolff, D. J. Grimwood, D. Jayatilaka, M. A. Spackman, *J. Appl. Crystallogr.* **2021**, *54*, 1006–1011.
[58] C. F. Macrae, P. R. Edgington, P. McCabe, E. Pidcock, G. P. Shields, R. Taylor, M. Towler, J. van de Streek, *J. Appl. Crystallogr.* **2006**, *39*, 453–457.
[59] a) D. J. Cole, J. Z. Vilseck, J. Tirado-Rives, M. C. Payne, W. L. Jorgensen, *J. Chem. Theory Comput.* **2016**, *12*, 2312–2323; b) A. E. A. Allen, M. C. Payne, D. J. Cole, *J. Chem. Theory Comput.* **2018**, *14*, 274–281; c) J. T. Horton, A. E. A. Allen, L. S. Dodda, D. J. Cole, *J. Chem. Inf. Model.* **2019**, *59*, 1366–1381; d) C. Ringrose, J. T. Horton, L.-P. Wang, D. J. Cole, *Phys. Chem. Chem. Phys.* **2022**, *24*, 17014–17027.
[60] a) F. Weigend, *Phys. Chem. Chem. Phys.* **2006**, *8*, 1057–1065; b) F. Neese, *WIREs Comput. Mol. Sci.* **2012**, *2*, 73–78; c) S. Lehtola, C. Steigemann, M. J. T. Oliveira, M. A. L. Marques, *SoftwareX* **2018**, *7*, 1–5; d) F. Neese, *WIREs Comput. Mol. Sci.* **2022**, *12*, e1606.
[61] E. F. Valeev, *Libint: A library for the evaluation of molecular integrals of many-body operators over Gaussian functions*, http://libint.valeyev.net/, **2024**.
[62] R. F. W. Bader, *Acc. Chem. Res.* **1985**, *18*, 9–15.
[63] T. Lu, F. Chen, *J. Comput. Chem.* **2012**, *33*, 580–592.
[64] a) C. Lee, W. Yang, R. G. Parr, *Phys. Rev. B* **1988**, *37*, 785–789; b) A. D. Becke, *J. Chem. Phys.* **1993**, *98*, 1372–1377.
[65] M. J. Abraham, T. Murtola, R. Schulz, S. Páll, J. C. Smith, B. Hess, E. Lindahl, *SoftwareX* **2015**, *1–2*, 19–25.
[66] D. Horinek, S. I. Mamatkulov, R. R. Netz, *J. Chem. Phys.* **2009**, *130*, 124507.
[67] a) R. Ahlrichs, M. Bär, M. Häser, H. Horn, C. Kölmel, *Chem. Phys. Lett.* **1989**, *162*, 165–169; b) K. Eichkorn, O. Treutler, H. Öhm, M. Häser, R. Ahlrichs, *Chem. Phys. Lett.* **1995**, *240*, 283–290; c) K. Eichkorn, F. Weigend, O. Treutler, R. Ahlrichs, *Theor. Chem. Acc.* **1997**, *97*, 119–124; d) M. V. Arnim, R. Ahlrichs, *J. Comput. Chem.* **1998**, *19*, 1746–1757; e) M. Sierka, A. Hogekamp, R. Ahlrichs, *J. Chem. Phys.* **2003**, *118*, 9136–9148; f) P. Deglmann, K. May, F. Furche, R. Ahlrichs, *Chem. Phys. Lett.* **2004**, *384*, 103–107.
[68] S. Grimme, J. Antony, S. Ehrlich, H. Krieg, *J. Chem. Phys.* **2010**, *132*, 154104.
[69] a) F. Weigend, R. Ahlrichs, *Phys. Chem. Chem. Phys.* **2005**, *7*, 3297–3305; b) F. Weigend, *Phys. Chem. Chem. Phys.* **2006**, *8*, 1057–1065; c) F. Weigend, *J. Comput. Chem.* **2008**, *29*, 167–175; d) D. Rappoport, F. Furche, *J. Chem. Phys.* **2010**, *133*, 134105.
[70] a) A. Klamt, G. Schüürmann, *J. Chem. Soc. Perkin Trans. 2* **1993**, 799–805; b) A. Klamt, V. Jonas, *J. Chem. Phys.* **1996**, *105*, 9972–9981; c) A. Klamt, C. Moya, J. Palomar, *J. Chem. Theory Comput.* **2015**, *11*, 4220–4225; d) A. Klamt, M. Diedenhofen, *J. Comput. Chem.* **2018**, *39*, 1648–1655.
[71] R. D. Dennington II, T. A. Keith, J. M. Millam, *GaussView 5.0*; Gaussian, Inc.: Wallingford, CT, USA, **2008**.
[72] J. B. Foresman, A. Frisch, *Exploring Chemistry with Electronic Structure Methods*, 2nd Ed.; Gaussian, Inc.: Pittsburgh, PA, USA, **1996**.

Manuscript received: December 20, 2024
Accepted manuscript online: January 27, 2025
Version of record online: ■■, ■■

Research Article

Hydrogen Bonding

T. Huber, G. Mayer, M. Kümper, W. Silva, N. Fontana, A. Falk, S. H. F. Schreiner, J. Gramüller, A. Scrimgeour, E. Groß, R. M. Gschwind, D. Horinek, P. Nuernberger, J. O. Bauer* _____ **e202425049**

Where Does the Proton Go? Structure and Dynamics of Hydrogen-Bond Switching in Aminophosphine Chalcogenides

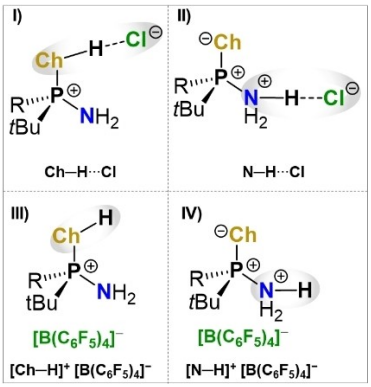

Aminophosphine chalcogenides are relevant in many organocatalytic concepts and are the focus of prebiotic studies. Spectroscopy (IR, ^{1}H DOSY, ^{15}N NMR), MD simulations, and DFT calculations provide unique insight into their proton-binding affinity. All conceivable hydrogen-bonding modes can be formed and controlled. Fundamental principles of self-organization, proton-hopping, and of the behavior at the lower concentration threshold are revealed.